1 **Nocturnal Atmospheric Synergistic Oxidation Reduces the Formation of Low-volatility**

2 **Organic Compounds from Biogenic Emissions**

3 Han Zang[1], Zekun Luo[1], Chenxi Li[1], Ziyue Li[1], Dandan Huang[2,*], Yue Zhao[1,*]

5 [1]School of Environmental Science and Engineering, Shanghai Jiao Tong University, Shanghai,

6 200240, China

7 [2]Shanghai Academy of Environmental Sciences, Shanghai, 200233, China

8 *Correspondence: Yue Zhao (yuezhao20@sjtu.edu.cn); Dandan Huang (huangdd@saes.sh.cn);

10 **Abstract**

11 Volatile organic compounds (VOCs) are often subject to synergistic oxidation by different oxidants

12 in the atmosphere. However, the exact synergistic oxidation mechanism of atmospheric VOCs and

13 its role in particle formation remain poorly understood. In particular, the reaction kinetics of the key

14 reactive intermediates, organic peroxy radicals (RO_2), during synergistic oxidation is rarely studied.

15 Here, we conducted a combined experimental and kinetic modelling study of the nocturnal

16 synergistic oxidation of α-pinene (the most abundant monoterpene) by O_3 and NO_3 radicals as well

17 as its influences on the formation of highly oxygenated organic molecules (HOMs) and particles.

18 We find that in the synergistic $O_3 + NO_3$ regime, where OH radicals are abundantly formed via

19 decomposition of ozonolysis-derived Criegee intermediates, the production of $C_xH_yO_z$-HOMs is

20 substantially suppressed compared to that in the O_3-only regime, mainly because of the termination

21 of α-pinene RO_2 derived from ozonolysis and OH oxidation by those arising from NO_3 oxidation.

22 Measurement-model comparisons further reveal that the termination reactions between ozonolysis-

23 and NO_3-derived RO_2 are on average $10 - 100$ times more efficient than those of OH- and NO_3-

24 derived RO_2. Despite a strong production of organic nitrates in the synergistic oxidation regime, the

25 substantial decrease of $C_xH_yO_z$-HOM formation leads to a significant reduction in ultralow- and

26 extremely low-volatility organic compounds, which significantly inhibits the formation of new

27 particles. This work provides valuable mechanistic and quantitative insights into the nocturnal

28 synergistic oxidation chemistry of biogenic emissions and will help to better understand the

29 formation of low-volatility organic compounds and particles in the atmosphere.

30

1. Introduction

The Earth's atmosphere is a complex oxidizing environment in which multiple oxidants coexist. During the nighttime, NO_3 radicals (generated by the reaction of NO_2 and O_3) and O_3 contribute significantly to the oxidation of volatile organic compounds (VOCs) (Huang et al., 2019), while during the daytime, the fast photolysis of NO_3 radicals and rapid photochemical formation of OH radicals and O_3 make the latter two the major oxidants for VOCs (Zhang et al., 2018). Therefore, the degradation of ambient VOCs is subject to concurrent oxidation by different oxidants. Gas-phase oxidation of VOCs from biogenic emissions (BVOCs) by these major atmospheric oxidants produces a key type of reactive intermediates, organic peroxy radicals (RO_2), a portion of which can undergo fast autoxidation forming a class of highly oxygenated organic molecules (HOMs) with low volatilities (Jokinen et al., 2014; Mentel et al., 2015; Berndt et al., 2016; Zhao et al., 2018; Iyer et al., 2021; Shen et al., 2022; Ehn et al., 2014). HOMs typically contain six or more oxygen atoms, and plays a key role in the formation of atmospheric new particles and secondary organic aerosol (SOA) (Kirkby et al., 2016; Berndt et al., 2018; Zhao et al., 2018; Ehn et al., 2014; Bianchi et al., 2019), which have important influences on air quality (Huang et al., 2014), public health (Pye et al., 2021), and Earth's radiative forcing (Shrivastava et al., 2017).

Due to the complexity of oxidation mechanisms of BVOCs, previous laboratory studies typically featured only one oxidant and a single SOA precursor (Berndt et al., 2016; Berndt, 2021; Claflin et al., 2018; Iyer et al., 2021; Boyd et al., 2015). However, the synergistic oxidation by different oxidants may significantly alter the fate of RO_2 intermediates, therefore influencing the formation of HOMs and SOA (Bates et al., 2022). Recently, a field study at a boreal forest site in Finland observed a series of nitrate-containing HOM-dimers from the coupled O_3 and NO_3 oxidation of monoterpenes (Zhang et al., 2020). At the same site, Lee et al. (2020) found that the synergistic oxidation of BVOCs by OH radicals and O_3 contributed to the largest fraction of SOA. These studies suggest that the synergistic oxidation of BVOCs by different oxidants plays an important role in the formation of HOMs and SOA in the atmosphere and highlight the needs to investigate the synergistic oxidation mechanisms of BVOCs for a better representation of atmospheric particle formation.

Several laboratory studies have attempted to address the role of synergistic oxidation of BVOCs in the formation of new particles and SOA (Kenseth et al., 2018; Inomata, 2021; Liu et al., 2022; Li et

60 al., 2024). Kenseth et al. (2018) identified a suite of dimer esters in flow tube experiments that can

61 be only formed from the OH and O_3 synergistic oxidation of β-pinene. These dimers exhibit

62 extremely low volatility and contributed 5.9 – 25.4% to the total β-pinene SOA. Similarly, Inomata

63 (2021) found that the presence of OH radicals during α-pinene ozonolysis is a key factor for the

64 production of low-volatility organic species and significantly promotes new particle formation

65 (NPF). On the other hand, the addition of O_3 in the monoterpene photooxidation system also

66 significantly increases the SOA mass yield (Liu et al., 2022). In addition, a recent chamber study

67 by Bates et al. (2022) showed that the synergistic oxidation of α-pinene by NO_3 radicals and O_3 can

68 significantly enhance the SOA yield compared to the NO_3 + α-pinene regime, which has nearly 0%

69 SOA yield (Fry et al., 2014; Hallquist et al., 1999; Mutzel et al., 2021), and they revealed that the

70 SOA yield in the NO_3 + O_3 oxidation system largely depends on the RO_2 fates. Most recently, Li et

71 al. (2024) found that during α-pinene ozonolysis, the presence of nitrooxy-RO_2 radicals formed from

72 NO_3 oxidation can significantly suppress the production of ultralow-volatility organic compounds

73 (ULVOCs) and thereby NPF. These laboratory studies together provide growing evidence that

74 synergistic oxidation of BVOCs by different oxidants have profound impacts on atmospheric

75 particle formation. However, the specific synergistic mechanisms of different oxidants and

76 oxidation pathways remain obscure. Although a few studies underscored the importance of the RO_2

77 fates (Bates et al., 2022; Li et al., 2024), the exact interactions between RO_2 species derived from

78 different oxidants are still unclear, and quantitative constraints on the reaction rate of different RO_2

79 species are quite limited.

80 Here we conducted an investigation of the synergistic O_3 + NO_3 oxidation of α-pinene, one of the

81 most abundant monoterpenes in the atmosphere, using a combination of laboratory experiments and

82 detailed kinetic modelling, and focusing on the fate of RO_2 intermediates arising from different

83 oxidation pathways. The α-pinene oxidation experiments were conducted in a custom-built flow

84 reactor. The molecular composition of RO_2 species and HOMs in different oxidation regimes was

85 characterized using a chemical ionization atmospheric pressure interface time-of-flight mass

86 spectrometer (CI-APi-ToF) employing a nitrate ion source. The measured distributions of specific

87 RO_2 and HOMs across different oxidation regimes were fitted with a kinetic model using Master

88 Chemical Mechanisms (MCM v3.3.1) updated with recent advances of α-pinene RO_2 chemistry

89   (Wang et al., 2021; Iyer et al., 2021; Shen et al., 2022; Zang et al., 2023), which allows for

90   quantitative constraints on RO_2 kinetics and synergistic oxidation mechanisms. Atmospheric

91   relevance of the experimental results was evaluated by modelling the investigated oxidation

92   chemistry under typical nocturnal atmospheric conditions.

93   **2. Materials and Methods**

94   **2.1 Flow Tube Experiments**

95   Experiments of α-pinene oxidation in different regimes (i.e., synergistic $O_3 + NO_3$ oxidation vs. O_3-

96   only) were carried out under room temperature (298 K) and dry (relative humidity < 5%) conditions

97   in a custom-built flow tube reactor (FTR, Figure S1). O_3 and NO_2 were added into a glass tube

98   (Figure S1) to form NO_3 radical and its precursor N_2O_5:

99    $NO_2 + O_3 \rightarrow NO_3 + O_2$ (R1)

100    $NO_3 + NO_2 \leftrightarrow N_2O_5$ (R2)
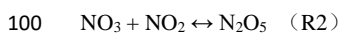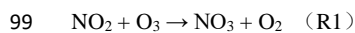
101   O_3 was generated by passing a flow of ultra-high-purity (UHP) O_2 (Shanghai Maytor Special Gas

102   Co., Ltd.) through a quartz tube housing a pen-ray mercury lamp (UV-S2, UVP Inc.) and its

103   concentration was measured by an ozone analyzer (T400, API). NO_2 was obtained from a gas

104   cylinder (15.6 ppm, Shanghai Weichuang Standard Gas Co., Ltd.). The total air flow in the NO_3

105   generation glass tube was 0.6 L min^{-1} and 0.4 L min^{-1} for the gas-phase HOM and SOA formation

106   experiments, respectively. The produced N_2O_5 and NO_3 radicals, as well as the excessive O_3 were

107   added into the FTR to initiate α-pinene oxidation. For the O_3-only experiments, only O_3 was added

108   into FTR.

109   The α-pinene gas was generated by evaporating a defined volume of their liquid (99%, Sigma-

110   Aldrich) into a cleaned and evacuated canister (SilcoCan, RESTEK), and then added into FTR

111   through a movable injector at a flow rate of 22 – 108 mL min^{-1}. The initial concentration of α-pinene

112   in the flow reactor ranged from 100 – 500 ppb. In some experiments, the gas of cyclohexane (~ 100

113   ppm), which was generated by bubbling a gentle flow of UHP N_2 through its liquid (LC-MS grade,

114   CNW), was added into the flow reactor as a scavenger of OH radicals formed from α-pinene

115   ozonolysis.

116   For experiments characterizing the formation of HOMs, the total air flow in the FTR was 10.8 L

117   min⁻¹ and the residence time was 25 seconds. The short reaction time and the small amount of

118   reacted α-pinene (see Table S1) in these experiments prevented the formation of particles. For the

119   experiments characterizing the formation of SOA particles, a larger FTR was used, with a total air

120   flow of 5 L min⁻¹ and a residence time of 180 seconds. A summary of the conditions including the

121   simulated concentrations of N_2O_5 and NO_3 radicals in different experiments are shown in Table S1.

122   The gas-phase RO_2 radicals and closed-shell products were measured using a nitrate-based CI-APi-

123   ToF (abbreviated as nitrate-CIMS; Aerodyne Research, Inc.), which has been described in detail

124   previously (Zang et al., 2023). A long ToF-MS with a mass resolution of ~10000 Th/Th was used

125   here. The mass spectra within the m/z range of 50-700 were analyzed using the tofTools package

126   developed by Junninen et al. (2010) based on Matlab. A scanning mobility particle sizer (SMPS,

127   TSI), consisting of an electrostatic classifier (model 3082), a differential mobility analyzer (model

128   3081), and a condensation particle counter (model 3756), was employed to monitor the formation

129   of particles in different oxidation experiments.

130   **2.2 Estimation of HOM Volatility**

131   A modified composition-activity method was used to estimate the saturation mass concentration

132   (C^*) of HOMs in this study according to the approach developed by Li et al. (2016):

133   $$\log_{10}C^* = (n_C^0 - n_C)b_C - n_O b_O - 2\frac{n_C n_O}{n_C + n_O}b_{co} - n_N b_N - n_S b_S$$

134   where n_C^0 is the reference carbon number; n_C, n_O, n_N, and n_S are the atom numbers of carbon,

135   oxygen, nitrogen, and sulfur, respectively; b_C, b_O, b_N, and b_S are the contribution of each atom

136   to $\log_{10}C^*$, respectively; b_{co} is the carbon–oxygen nonideality (Donahue et al., 2011). These b-

137   values were provided by Li et al. (2016).

138   It should be noted that the CHON compounds used in the data set by Li et al. (2016) are mostly

139   amines, amides, and amino acids, and only contain a limited number of organic nitrates (0.07%).

140   Since different types of CHON compounds have very different vapor pressures (Isaacman-Vanwertz

141   and Aumont, 2021), this formula-based approach can be biased to estimate the C^* of organic nitrates.

142   Considering that the –ONO_2 and –OH groups have similar impacts on vapor pressure and that the

143   CHON species are predominantly organic nitrates in our study, all –ONO_2 groups are treated as OH

144   groups during the estimation of vapor pressure (Daumit et al., 2013; Isaacman-Vanwertz and

145   Aumont, 2021).

146   Gas-phase HOMs are grouped into five classes based on their $\log_{10}C^*$ (Donahue et al., 2012;

147   Bianchi et al., 2019; Schervish and Donahue, 2020), that is, ULVOCs ($\log_{10}C^* < -8.5$), extremely

148   low-volatility organic compounds (ELVOCs, $-8.5 < \log_{10}C^* < -4.5$), low-volatility organic

149   compounds (LVOCs, $-4.5 < \log_{10}C^* < -0.5$), semi-volatile organic compounds (SVOCs, $-0.5 <$

150     $\log_{10}C^* < 2.5$), and intermediate-volatility organic compounds (IVOCs, $2.5 < \log_{10}C^* < 6.5$).

151   **2.3 Kinetic Model Simulations**

152   Model simulations of specific RO_2 radicals and closed-shell HOMs formed in different oxidation

153   regimes were performed to constrain the reaction kinetics and mechanisms using the Framework

154   for 0-D Atmospheric Modeling (F0AM v4.1) (Wolfe et al., 2016), which employs MCM v3.3.1

155   (Jenkin et al., 2015). The α-pinene oxidation mechanism was updated with the state-of-the-art

156   knowledge on the chemistry of RO_2 autoxidation and cross-reactions forming HOM monomers and

157   dimers, respectively (Zhao et al., 2018; Wang et al., 2021; Iyer et al., 2021; Shen et al., 2022). The

158   detailed updates have been described in our previous study (Zang et al., 2023). In particular, the

159   formation and subsequent reactions of the ring-opened primary $C_{10}H_{15}O_4$-RO_2, the highly

160   oxygenated acyl RO_2, as well as the $C_{10}H_{15}O_2$-RO_2 arising from H-abstraction by OH radicals

161   during α-pinene ozonolysis are included in the model according to recent studies (Iyer et al., 2021;

162   Zhao et al., 2022; Zang et al., 2023; Shen et al., 2022). To investigate the synergistic reactions of

163   RO_2 derived from the oxidation of α-pinene by different oxidants, we added the cross-reactions of

164   the primary nitrooxy-RO_2 derived from NO_3 oxidation ($^{NO3}RO_2$) with RO_2 derived from ozonolysis

165   ($^{CI}RO_2$) and OH oxidation ($^{OH}RO_2$). The cross-reaction rate constants of $^{NO3}RO_2 + {}^{CI}RO_2$ and

166     $^{NO3}RO_2 + {}^{OH}RO_2$ and their ratios were tuned to achieve a good measurement-model agreement for

167   the distribution of specific RO_2 and HOMs in the synergistic oxidation regime. The ROOR' dimer

168   formation rates for these RO_2 radicals were assumed to be the same as their cross-reaction rates.

169   Previous studies indicated that the primary $^{NO3}RO_2$ radicals arising from α-pinene are prone to lose

170   the nitrate group and form pinonaldehyde with high volatility (Kurtén et al., 2017; Fry et al., 2014).

171   Therefore, we did not consider the autoxidation of primary $^{NO3}RO_2$ in the model. Considering the

172   presence of NO_2 in the experiments, the reactions of $RO_2 + NO_2 \leftrightarrows ROONO_2$ were also included in

173   the model (Zang et al., 2023).

3. Results and Discussion

3.1 Molecular distribution of RO_2 and HOMs in the synergistic oxidation regime

The relative changes in the abundance of gas-phase RO_2 species and $C_xH_yO_z$-HOMs in the synergistic $O_3 + NO_3$ oxidation of α-pinene vs. the O_3-only regime are shown in Figure 1. The signals of $C_xH_yO_z$-HOMs significantly decrease by 29 – 36% in the synergistic $O_3 + NO_3$ regime compared to those in the O_3-only regime (Figure 1a). Note that the initial concentrations of α-pinene and O_3 in the two oxidation regimes were the same. In addition, model simulations show that in the synergistic oxidation regime, over 97% of OH radicals react with α-pinene and the depletion of OH by NO_2 is minor (0.2 – 1.3%). Also, NO_3 radicals almost entirely (over 98.5%) react with α-pinene and their reaction with RO_2 has negligible influence on the fate of RO_2. Therefore, the strong reduction in HOM formation in the synergistic oxidation regime vs. the O_3-only regime is likely due to the following two reasons. The first one is the fast competitive consumption of α-pinene by NO_3 radicals, which results in a reduction in the reacted α-pinene by O_3 (Δ[α-pinene]$_{O_3}$, Figure S2) and thereby the formation of $C_xH_yO_z$-HOMs. The second reason is associated with the reactions of $^{NO3}RO_2$ with $^{CI}RO_2$ or $^{OH}RO_2$ from α-pinene, which suppresses the autoxidation and self/cross-reactions of $^{CI}RO_2$ and $^{OH}RO_2$ to form $C_xH_yO_z$-HOMs.

To quantify the contribution of the synergistic RO_2 chemistry to the suppression of $C_xH_yO_z$-HOM formation in the $O_3 + NO_3$ oxidation regime, the $C_xH_yO_z$-HOM signal ratios in Figure 1a are further normalized to the ratio of Δ[α-pinene]$_{O_3}$ in the synergistic oxidation regime vs. the O_3-only regime (see Figure 1b). Notably, after excluding the influence of reduced Δ[α-pinene]$_{O_3}$, the $C_xH_yO_z$-HOMs signals still drop by 24 – 32% in the $O_3 + NO_3$ regime compared to those in the O_3-only regime, indicating a significant contribution of the coupled reactions between $^{NO3}RO_2$ and $^{CI}RO_2$ or $^{OH}RO_2$ to suppressed $C_xH_yO_z$-HOM formation.
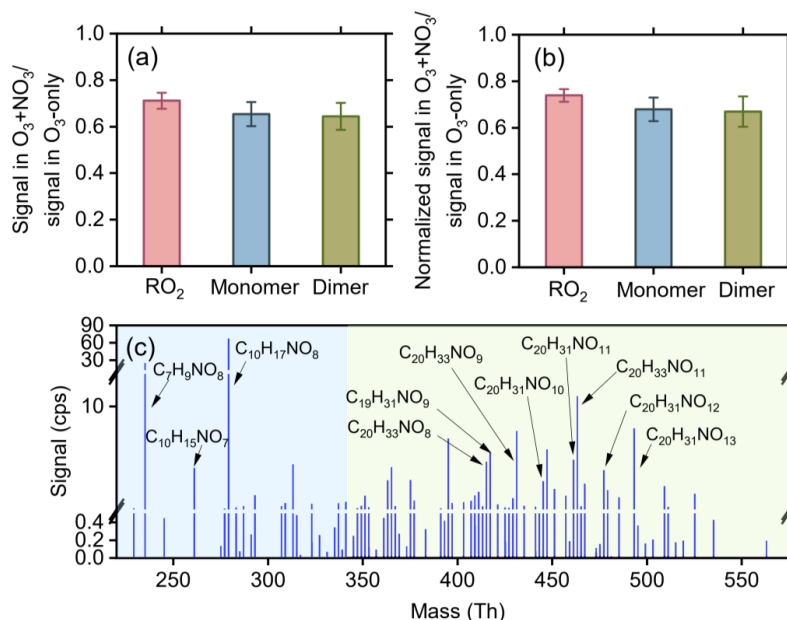
Figure 1. Distributions of RO_2 and HOMs in the synergistic $O_3 + NO_3$ regime. (a) Relative changes in the signals of $C_xH_yO_z$-RO_2 radicals, HOM monomers, and HOM dimers in the $O_3 + NO_3$ regime compared to those in the O_3-only regime (Exps 1-10). (b) Similar to (a), but with ion signals normalized to Δ[α-pinene]$_{O3}$ in each oxidation regime. (c) HOM nitrates measured in the $O_3 + NO_3$ regime.

Figure 1c shows the signals of closed-shell monomeric and dimeric HOM nitrates (HOM-ONs) that were only observed in the synergistic $O_3 + NO_3$ regime. Their specific formulas are listed in Table S2. These HOM-ONs mainly consist of C_{10} monomers and C_{20} dimers that only contain one nitrogen atom. The C_{20} HOM-ONs are believed to be formed from the cross-reactions of $^{Cl}RO_2$ and $^{OH}RO_2$ with $^{NO3}RO_2$. The substantial formation of these dimeric ONs provides direct evidence for the synergistic RO_2 chemistry in the $O_3 + NO_3$ regime. It should be noted that although several closed-shell monomeric HOM-ONs have been observed, only a few of them exhibit relatively high signals. In addition, no obvious signals of highly oxygenated $^{NO3}RO_2$ ($C_{10}H_{16}NO_x$, $x \geq 6$) were observed by nitrate-CIMS in the synergistic $O_3 + NO_3$ oxidation system. Previous studies revealed that the primary $^{NO3}RO_2$ radicals (i.e., $C_{10}H_{16}NO_5$-RO_2) in the α-pinene + NO_3 system mainly react to form pinonaldehyde (Kurtén et al., 2017; Perraud et al., 2010). Therefore, it is likely that only a very small amount of $^{NO3}RO_2$ can undergo autoxidation to form highly oxygenated $^{NO3}RO_2$. In addition, the overlapping of the $^{NO3}RO_2$ peaks with strong $C_xH_yO_z$-HOMs peaks also hinders the observation

216   of highly oxygenated $^{NO3}RO_2$ signals in this study (Table S3). However, we note that although the

217   primary $C_{10}H_{16}NO_5$-RO_2 species arising from NO_3 oxidation may not undergo fast autoxidation,

218   they tend to efficiently terminate $^{Cl}RO_2$ and/or $^{OH}RO_2$ and suppress the formation of $C_xH_yO_z$-HOMs.

3.2 Synergistic reaction efficiencies of different RO$_2$ species

220   In the $O_3 + NO_3$ regime, synergistic reactions are likely to occur between $^{Cl}RO_2$, $^{OH}RO_2$ and $^{NO3}RO_2$.

221   Figure 2 shows the $\Delta[\alpha\text{-pinene}]_{O3}$-normalized signal ratios of specific C_{10} RO_2 as well as their

222   related $C_xH_yO_z$-HOM monomers and dimers in the synergistic $O_3 + NO_3$ regime vs. the O_3-only

223   regime. Model simulations show that the H-abstraction of α-pinene by OH radicals contributes less

224   than 2% to the formation of $C_{10}H_{15}O_x$-RO_2 and related HOMs under different experimental

225   conditions (Figure S3). Therefore, $C_{10}H_{15}O_x$-RO_2 observed in this study are primarily $^{Cl}RO_2$.

226   Notably, the $^{Cl}RO_2$ ($C_{10}H_{15}O_x$) and related $C_{10}H_{14}O_x$-HOMs decrease by $\sim30 - 60\%$ in the $O_3 + NO_3$

227   regime (Figures 2 a, b), while the decreasing extent of $^{OH}RO_2$ ($C_{10}H_{17}O_x$) and related $C_{10}H_{18}O_x$-

228   HOMs are significantly smaller ($0 - 40\%$). In particular, some of the most oxygenated $C_{10}H_{17}O_x$-

229   RO_2 and $C_{10}H_{18}O_x$-HOMs ($x \geq 9$) even increase unexpectedly in the synergistic oxidation regime.

230   For the $C_{10}H_{16}O_x$-HOMs that can be derived from the termination reactions of both $^{Cl}RO_2$ and

231    $^{OH}RO_2$, their reductions are at a medium level. The significantly larger decrease in signals of $^{Cl}RO_2$

232   and related HOMs as compared to the OH-derived ones indicates that in the synergistic $O_3 + NO_3$

233   regime, the $^{NO3}RO_2$ species have a strong termination effect on $^{Cl}RO_2$ than on $^{OH}RO_2$ (especially for

234   the most oxygenated $^{OH}RO_2$). Because a large amount of $^{Cl}RO_2$ is terminated by $^{NO3}RO_2$, fewer

235    $^{Cl}RO_2$ are available to terminate $^{OH}RO_2$. As a result, more $^{OH}RO_2$ can undergo autoxidation to form

236   highly oxygenated $C_{10}H_{17}O_x$-RO_2 and $C_{10}H_{18}O_x$-HOMs ($x \geq 9$), leading to an increase in signals of

237   these species. Consistently, the signals of C_{20} HOM dimers decrease by $20 - 40\%$ in the $O_3 + NO_3$

238   regime compared to that in O_3-only regime, and the signal reduction of dimers ($C_{20}H_{30}O_x$) formed

239   by $^{Cl}RO_2$ is slightly larger than that of the dimers ($C_{20}H_{34}O_x$) arising from $^{OH}RO_2$ (Figure 2c). Note

240   that the highly oxygenated $C_{20}H_{34}O_x$ dimers ($x \geq 13$) that can be formed from self/cross-reactions

241   of $C_{10}H_{17}O_x$-RO_2 ($x \geq 9$) are not observed in this study, likely due to their low abundance and the

242   limitation of instrument sensitivity.

243
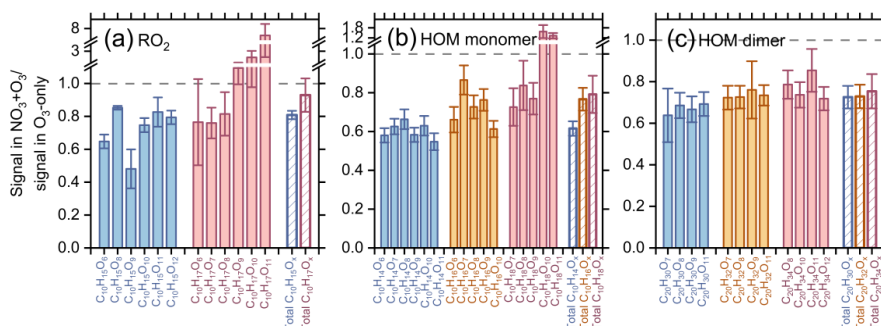
Figure 2. Normalized signal ratios of (a) specific and total $C_{10}H_{15,17}O_x$-RO_2 radicals, as well as their related (b) C_{10} HOM monomers and (c) C_{20} HOM dimers in the $O_3 + NO_3$ regime vs. the O_3-only regime (Exps 1-10). Ion signals observed in each oxidation regime are normalized to $\Delta[\alpha\text{-pinene}]_{O3}$.

To gain quantitative constraints on the relative reaction efficiency of $^{NO3}RO_2 + {}^{CI}RO_2$ vs. $^{NO3}RO_2 + {}^{OH}RO_2$ (i.e., k_{NO3+CI}/k_{NO3+OH}), the signal ratios of C_{10}-$^{CI}RO_2$ and $^{OH}RO_2$ as well as their related C_{10} HOMs in the synergistic oxidation regime vs. the O_3-only regime were predicted using a kinetic model (see Section 2.3) with different k_{NO3+CI}/k_{NO3+OH} ratios. Figure 3 shows a measurement-model comparison of those signal ratios. When the ratio of k_{NO3+CI}/k_{NO3+OH} is smaller than or equal to 1, the simulated signal ratios of many RO_2 and HOMs differ significantly from the measured ratios, especially for some $C_{10}H_{17}O_x$-RO_2 and $C_{10}H_{18}O_x$-HOMs. When the ratio of k_{NO3+CI}/ k_{NO3+OH} is 10 – 100, there is a good measurement-model agreement for most of RO_2 and HOMs. Therefore, we conclude that the cross-reactions of $^{NO3}RO_2 + {}^{CI}RO_2$ are on average 10 – 100 times more efficient than $^{NO3}RO_2 + {}^{OH}RO_2$.

As a competitive reaction pathway, the autoxidation rates of RO_2 can affect the extent to which RO_2 cross-reactions influence the RO_2 fate and HOM formation. Therefore, sensitivity analyses of the autoxidation rate of RO_2 were conducted to evaluate its influence on the changes of RO_2 and related HOM concentrations in the synergistic $O_3 + NO_3$ regime vs. the O_3-only regime (Figure S4). In these analyses, a k_{NO3+CI}/k_{NO3+OH} ratio of 10 was used according to the above discussions. As the autoxidation rate of $^{OH}RO_2$ increases from 0.28 to 10 s^{-1}, corresponding to the rate range reported in previous studies (Berndt et al., 2016; Zhao et al., 2018; Xu et al., 2019), the simulated reduction of highly oxygenated $^{OH}RO_2$ and related $C_{10}H_{18}O_x$-HOMs in the synergistic $O_3 + NO_3$ regime exhibits a slight decrease (< 7%) but still agrees reasonably well with the measured value (Figures S4 a-d). Considering that the autoxidation rates of $^{CI}RO_2$ used in the model approach their upper limits

268   reported in the literature, i.e., ~1 s^{-1} for the butyl ring-opened $C_{10}H_{15}O_4$-RO_2 (Iyer et al., 2021) and

269   relatively smaller rates for ring-retained $C_{10}H_{15}O_4$-RO_2 (0.02 – 0.29 s^{-1}, see Scheme S1) (Zhao et

270   al., 2021), we also lowered the autoxidation rate constants of $^{Cl}RO_2$ by a factor of 10 to see its

271   influence on RO_2 and HOM distribution in the $O_3 + NO_3$ regime. The simulated reduction of $^{Cl}RO_2$

272   and $C_{10}H_{14}O_x$-HOMs in this case decreases by 11 – 18% (Figures S4 e-h), while that of $C_{10}H_{16}O_x$-

273   HOMs increases by up to 30% (Figures S4 i, j). However, the simulated results are still close to the

274   measured values. These sensitivity analyses suggest that the uncertainty in the autoxidation rates of

275     $^{OH}RO_2$ and $^{Cl}RO_2$ could slightly affect the simulated distribution of RO_2 and HOMs across different

276   oxidation regimes but not significantly change the k_{NO3+Cl}/k_{NO3+OH} ratio obtained in this study.
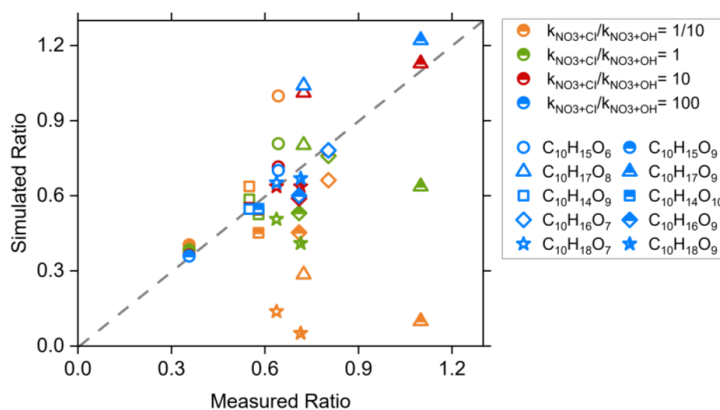
277

278   Figure 3. Measurement-model comparisons of the signal ratios of different C_{10} RO_2 and HOMs in

279   the synergistic $O_3 + NO_3$ regime vs. the O_3-only regime. The cross-reaction rate of $^{NO3}RO_2 + ^{Cl}RO_2$

280   was set to 1×10^{-12} cm^3 molecule^{-1} s^{-1} and the rate of $^{NO3}RO_2 + ^{OH}RO_2$ was varied from 1×10^{-11} cm^3

281   molecule^{-1} s^{-1} to 1×10^{-14} cm^3 molecule^{-1} s^{-1} in the model.

282   Cyclohexane was added in some experiments as an OH scavenger to elucidate the role of $^{OH}RO_2$

283   chemistry in HOM formation in the $O_3 + NO_3$ regime. In the presence of cyclohexane, $^{OH}RO_2$

284   ($C_{10}H_{17}O_x$) and related HOM monomers ($C_{10}H_{18}O_x$) and dimers ($C_{20}H_{32}O_x$ and $C_{20}H_{34}O_x$) decrease

285   by more than 80% (Figure 4), while $^{Cl}RO_2$ ($C_{10}H_{15}O_x$) and related HOM monomers ($C_{10}H_{14}O_x$) and

286   dimers ($C_{20}H_{30}O_x$) only decrease slightly (< 30%), in a good agreement with previous measurements

287   (Zhao et al., 2018; Zang et al., 2023). The $C_{10}H_{16}O_x$ species, which can arise from both $^{Cl}RO_2$ and

288     $^{OH}RO_2$, exhibit a medium reduction (Figure 4b). It is interesting to note that with the addition of

289   cyclohexane, there is a significant increase in $C_{20}H_{31}NO_x$, which are formed from the cross-reactions

290   of $^{Cl}RO_2$ with $^{NO3}RO_2$. Such an enhanced production of $C_{20}H_{31}NO_x$ as compared to the slightly

291   deceased formation of $C_{20}H_{30}O_x$ indicates that the cross-reaction of $^{Cl}RO_2 + {}^{NO3}RO_2$ is fast compared

292   to that of $^{Cl}RO_2 + {}^{Cl}RO_2$ and $^{Cl}RO_2 + {}^{OH}RO_2$. As a result, when the $^{OH}RO_2$ are depleted, the $^{Cl}RO_2$

293   that are supposed to react with $^{OH}RO_2$, efficiently react with $^{NO3}RO_2$ to form $C_{20}H_{31}NO_x$, leading to

294   the increase in $C_{20}H_{31}NO_x$ signals.
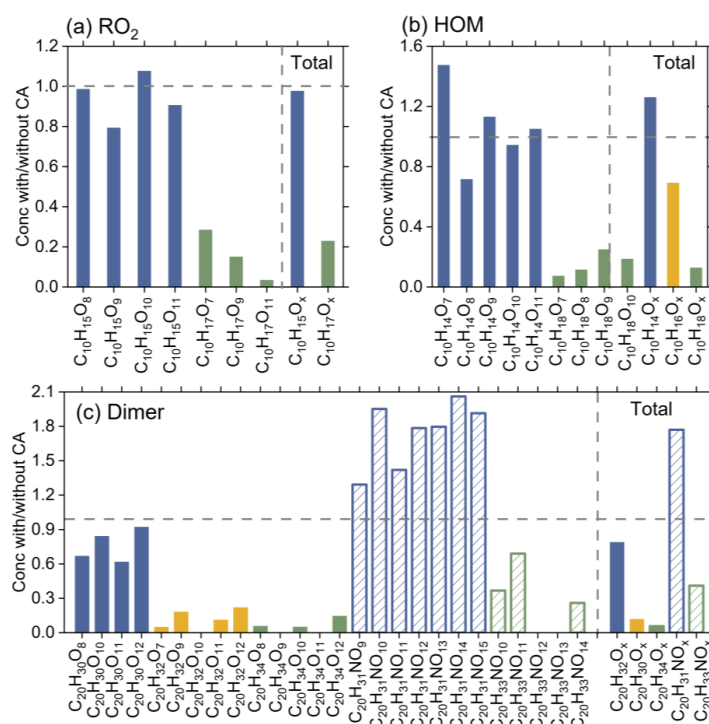
295

296   Figure 4. Relative changes in signals of (a) C_{10} RO_2, (b) C_{10} HOMs, and (c) C_{20} dimers due to the

297   addition of 100 ppm cyclohexane as an OH scavenger derived in the synergistic $O_3 + NO_3$ regime

298   (Exps 6 and 12).

299   **3.3 Influence of synergistic oxidation on low-volatility organics and particle formation**

300   Compared to the O_3-only regime, there is a remarkable reduction in $C_xH_yO_z$-HOMs and a strong

301   formation of HOM-ONs due to the termination reactions between $^{NO3}RO_2$ and $^{Cl}RO_2$ or $^{OH}RO_2$ in

302   the synergistic oxidation regime. This significant change in HOM composition and abundance

303   would alter the volatility distribution of HOMs and influence the formation of particles. The

304   volatilities of HOMs formed in the two oxidation regimes are estimated using a modified

305   composition-activity method (see Section 2.2) and shown in Figure 5. The abundance of $C_xH_yO_z$-

306   HOMs characterized as ULVOCs and ELVOCs decreases considerably in the synergistic $O_3 + NO_3$

307   regime compared to the O_3-only regime (Figure 5a), in agreement with the very recent observations

308   by Li et al. (2024) who found that the presence of NO_3 radicals during α-pinene ozonolysis

309   significantly reduced the abundance of ULVOCs. Although substantial amounts of HOM-ONs are

310   formed in the $O_3 + NO_3$ regime, they generally have higher volatilities (i.e., characterized as

311   ELVOCs to IVOCs) (Figure 5b). In addition, the total abundance of newly formed HOM-ONs

312   characterized as ELVOCs in the synergistic $O_3 + NO_3$ regime is significantly lower than the reduced

313   formation of ultra- and extremely low-volatility $C_xH_yO_z$-HOMs. Therefore, the synergistic $O_3 + NO_3$

314   oxidation of α-pinene significantly reduces the formation of ULVOCs and ELVOCs and increases

315   the overall volatility of total HOMs.
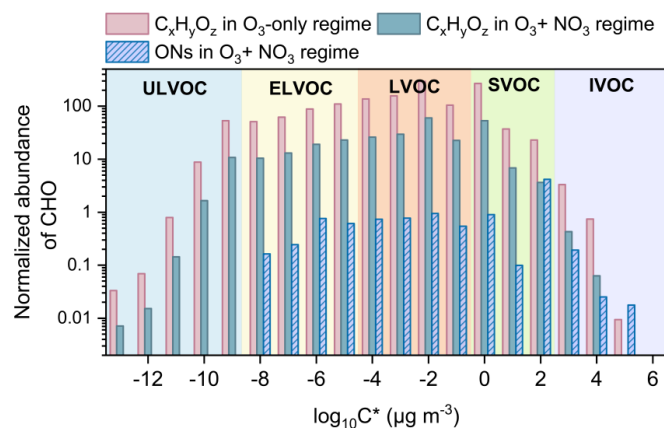
316

317   Figure 5. Volatility distribution of $C_xH_yO_z$-HOMs and HOM-ONs formed in the $O_3 + NO_3$ regime

318   and O_3-only regime (Exps 1, 6). Ion signals in each oxidation regime are normalized to the

319   corresponding total reacted α-pinene.

320   Figure 6 shows the particle number and mass concentrations formed in the two oxidation regimes

321   in SOA formation experiments (Table S1, Exps 13, 14). The particle number concentration decreases

322   by more than 50% whereas the particle mass concentration increases by a factor of 2 in the

323   synergistic $O_3 + NO_3$ regime, compared to that in the O_3-only regime. The reduced particle number

324   concentration in the $O_3 + NO_3$ regime is ascribed to the suppressed formation of ULVOCs, which

325   are the key species driving the particle nucleation (Simon et al., 2020; Schervish and Donahue,

326   2020). However, although the newly formed HOM-ONs with relatively higher volatilities are

327   inefficient in initiating particle nucleation, they are able to partition into the formed particles and

328   contribute significantly to the particle mass growth. This result is consistent with a recent chamber

329   study which found that the SOA mass concentration is much higher during α-pinene oxidation by

330     $O_3 + NO_3$ than during ozonolysis (Bates et al., 2022).
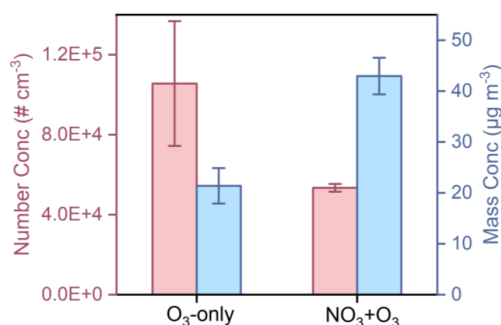
331

332   Figure 6. Number and mass concentrations of particles formed from the ozonolysis and synergistic

333     $O_3 + NO_3$ oxidation of α-pinene (Exps 13-14).

334   **3.4 Atmospheric relevance of experimental results**

335   To evaluate the relevance of our experimental findings to the real atmosphere, we performed

336   chemical model simulations of HOM formation from nocturnal synergistic $O_3 + NO_3$ oxidation of

337   α-pinene under typical atmospheric conditions. In these simulations, constant concentrations of α-

338   pinene (1 ppb), O_3 (30 ppb), NO (5 ppt), NO_2 (1.8 ppb), NO_3 radicals (0.2 or 1 ppt), OH radicals (5

339     $- 50 \times 10^4$ molecules cm^{-3}), HO_2 radicals (4 ppt), as well as a constant RH of 50% and temperature

340   of 298 K were used as typical nocturnal conditions in the boreal forest according to the field studies

341   (Stone et al., 2012; Lee et al., 2016; Brown and Stutz, 2012; Geyer et al., 2003b; Kristensen et al.,

342   2016; Hakola et al., 2012; Liebmann et al., 2018). Considering the rapid deposition of oxidized

343   biogenic compounds (Nguyen et al., 2015), a typical dilution lifetime of 5 h (i.e., $k_{dil} = 1/5$ h^{-1}) was

344   assumed in the model. According to the above analysis, the cross-reaction rate constants for $^{NO3}RO_2$

345   + $^{Cl}RO_2$ and $^{NO3}RO_2 + {}^{OH}RO_2$ were set to 1×10^{-12} cm^3 molecule^{-1} s^{-1} and 1×10^{-13} cm^3 molecule^{-1}

346   s^{-1} in the model, respectively.

347   As shown in Figure 7a, when a relatively low NO_3 concentration (0.2 ppt) is considered, ozonolysis

348   is the primary loss pathway of α-pinene (68%), followed by NO_3 (30%) and OH oxidation (2%).

349   The reactions of $RO_2 + HO_2$, $RO_2 + NO$ and $RO_2 + RO_2$ account for ~49%, ~27% and ~24% of the

350   total RO$_2$ fate, respectively. Under these conditions, the synergistic O$_3$ + NO$_3$ oxidation of α-pinene

351   leads to a reduction of 3% and 13% in the formation of C$_x$H$_y$O$_z$-HOM monomers and dimers,

352   respectively (Figure 7b). Given that the concentrations of α-pinene and oxidants were held constant

353   during the simulation, the consumptions of α-pinene by different oxidants are constant. Therefore,

354   the decreases in the concentrations of C$_x$H$_y$O$_z$-HOM monomers and dimers in the presence of NO$_3$

355   oxidation are mainly due to the cross-reaction of ^{NO3}RO$_2$ with other RO$_2$. When the NO$_3$

356   concentration is as high as 1 ppt as reported in field studies (Liebmann et al., 2018), NO$_3$ oxidation

357   contributes to 68% of α-pinene consumption (Figure 7c), and the contribution of RO$_2$ + RO$_2$ reaction

358   increases to 33%. As a result, the cross-reactions of ^{NO3}RO$_2$ with other RO$_2$ play a more important

359   role in the HOM formation. Under these conditions, the production of C$_x$H$_y$O$_z$-HOM monomers and

360   dimers decreases by 13% and 43%, respectively, due to the presence of NO$_3$ oxidation (Figure 7d).

361   Considering that there are uncertainties in the dilution rate constant, a sensitivity analysis was

362   performed by varying the k_{dil} in the range of 0.04 – 0.2 h^{-1}. It is found that the variation within these

363   rate values does not significantly influence the response of C$_x$H$_y$O$_z$-HOM dimer formation to

364   concurrent NO$_3$ oxidation (Figure S5).

365   Field observations have shown that NO$_3$ radicals, O$_3$, and OH radicals all had important

366   contributions to monoterpene oxidation during the early morning after sunrise and late afternoon

367   before sunset in the southeastern United States (Zhang et al., 2018). In addition, relatively high

368   nighttime OH concentrations of $(2 – 10) \times 10^5$ molecules cm^{-3} were measured in some areas such

369   as Germany and New York City (Faloona et al., 2001; Geyer et al., 2003a). As a result, model

370   simulations using the same species concentration (NO$_3$ = 1 ppt) as mentioned above but a 10 times

371   higher OH concentration $(5 \times 10^5$ molecules cm$^{-3})$ were also conducted. With a higher OH

372   concentration, O$_3$, NO$_3$, and OH radicals account for 28%, 62%, and 10% to the total α-pinene

373   consumption, respectively (Figure S6 a). Compared to the results under low OH concentration, the

374   formation of C$_x$H$_y$O$_z$-HOM monomers and dimers are all enhanced under high OH concentration

375   (Figure S6 b). This is mainly due to the promoted self/cross-reactions of ^{OH}RO$_2$, as well as the

376   promoted formation of C$_{10}$H$_{15}$O$_x$-RO$_2$ derived from H-abstraction pathway by OH radicals.

377   Nevertheless, the presence of NO$_3$ oxidation still reduces the formation of C$_x$H$_y$O$_z$-HOM dimers by

378   26% (Figure S6 b).

379   The above model simulations clearly suggest that under typical nocturnal atmospheric conditions,

380   the synergistic oxidation of α-pinene by O_3 and NO_3 radicals can significantly inhibit the formation

381   of $C_xH_yO_z$-HOMs, many of which are characterized as ULVOCs capable of driving particle

382   nucleation and initial growth. Although HOM-ON dimers are readily produced bycross-reactions

383   between $^{NO3}RO_2$ and $^{CI}RO_2$, they generally have higher volatilities than $C_xH_yO_z$-HOM dimers and

384   therefore are less efficient in initiating particle formation. Our results offer mechanistic and

385   quantitative insights on how the synergistic oxidation of α-pinene by O_3 and NO_3 radicals can

386   influence the formation of low-volatility organic compounds and hence particle formation and

387   growth. They also provide a potential explanation for field observations that NPF events frequently

388   occur in monoterpene-rich regions during daytime but not at nighttime (Mohr et al., 2017; Kulmala

389   et al., 2001; Junninen et al., 2017).
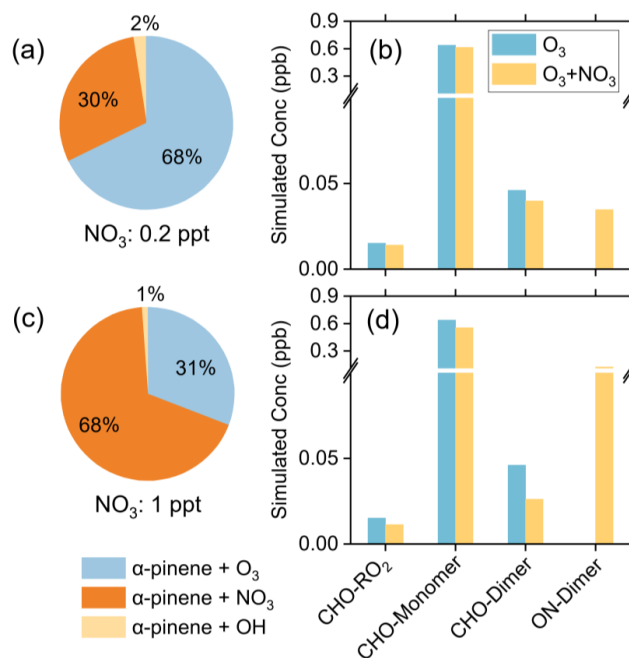
390

391   Figure 7. Model simulations of α-pinene oxidation and HOM formation under typical nighttime

392   conditions in the boreal forest. (a, c) Contributions of different loss pathways of α-pinene by

393   different oxidants at NO_3 concentrations of 0.2 and 1 ppt, respectively; (b, d) Concentrations of

394    $C_xH_yO_z$-HOMs and HOM-ONs formed by synergistic $O_3 + NO_3$ oxidation and ozonolysis of α-

395   pinene under conditions corresponding to (a) and (c). The simulations were run for 4 h after an 8-h

396   spin-up for intermediates and secondary species.

4. Conclusions

This study provides a comprehensive characterization of the nocturnal synergistic oxidation of α-pinene by O_3 and NO_3 radicals and its influence on the formation of HOMs and low-volatility organic compounds using a combination of flow reactor experiments and detailed kinetic model simulations. It is found that the formation of $C_xH_yO_z$-HOMs in the O_3 + NO_3 regime is significantly suppressed compared to that in the O_3-only regime, mainly due to the termination of ozonolysis-derived RO_2 (i.e., $^{CI}RO_2$ and $^{OH}RO_2$) by $^{NO3}RO_2$. In addition, the decreases in the abundance of $^{CI}RO_2$ and related HOMs are significantly larger than those of OH-derived ones, indicating that the $^{NO3}RO_2$ species have a strong termination effect on $^{CI}RO_2$ than on $^{OH}RO_2$. Detailed measurement-model comparisons for the distribution of a suite of $^{CI}RO_2$, $^{OH}RO_2$, and associated HOMs across different oxidation regimes further reveal that the terminations reactions between $^{CI}RO_2$ and $^{NO3}RO_2$ are averagely 10 – 100 times more efficient than those of $^{OH}RO_2$ and $^{NO3}RO_2$.

The suppressed formation of $C_xH_yO_z$-HOMs in the synergistic O_3 + NO_3 regime results in a significant reduction in ULVOCs. Although substantial amounts of HOM-ONs are formed from the cross-reactions between $^{NO3}RO_2$ and $^{CI}RO_2$ or $^{OH}RO_2$ in the synergistic oxidation regime, they have higher volatilities and are less likely to participate in the formation and initial growth of new particles. As a result, in our experiment the formation of new particles in the synergistic oxidation regime is substantially inhibited compared to the O_3-only regime. Chemical model simulations further confirm that the synergistic oxidation of α-pinene by O_3 and NO_3 radicals can significantly inhibit the formation of $C_xH_yO_z$-HOMs, especially the ultra-low volatility $C_xH_yO_z$-HOM dimers under typical nighttime atmospheric conditions. Our study sheds lights on the synergistic oxidation mechanism of biogenic emissions and underscores the importance of considering this chemistry for a better depiction of the formation of low-volatility organics and particles in the atmosphere.

Data availability. The data presented in this work are available upon request from the corresponding author.

Author contributions. YZ and HZ designed the study, HZ and DH performed the experiments. YZ and HZ analyzed the data, conducted model simulations, and wrote the paper. All other authors contributed to discussion and writing.

Competing interests. The authors declare no conflict of interest.

Acknowledgments. This work was supported by the National Natural Science Foundation of China (grants 22376137 and 22022607). Dan Dan Huang acknowledges the financial support from the Science and Technology Commission of Shanghai Municipality (grant 21230711000).

References

Bates, K. H., Burke, G. J. P., Cope, J. D., and Nguyen, T. B.: Secondary organic aerosol and organic nitrogen yields from the nitrate radical (NO_3) oxidation of alpha-pinene from various RO_2 fates, Atmos. Chem. Phys., 22, 1467-1482, 10.5194/acp-22-1467-2022, 2022.

Berndt, T.: Peroxy Radical Processes and Product Formation in the OH Radical-Initiated Oxidation of alpha-Pinene for Near-Atmospheric Conditions, J. Phys. Chem. A, 125, 9151-9160, 10.1021/acs.jpca.1c05576, 2021.

Berndt, T., Mentler, B., Scholz, W., Fischer, L., Herrmann, H., Kulmala, M., and Hansel, A.: Accretion Product Formation from Ozonolysis and OH Radical Reaction of alpha-Pinene: Mechanistic Insight and the Influence of Isoprene and Ethylene, Environ. Sci. Technol., 52, 11069-11077, 10.1021/acs.est.8b02210, 2018.

Berndt, T., Richters, S., Jokinen, T., Hyttinen, N., Kurtén, T., Otkjær, R. V., Kjaergaard, H. G., Stratmann, F., Herrmann, H., Sipilä, M., Kulmala, M., and Ehn, M.: Hydroxyl radical-induced formation of highly oxidized organic compounds, Nat. Commun., 7, 10.1038/ncomms13677, 2016.

Bianchi, F., Kurtén, T., Riva, M., Mohr, C., Rissanen, M. P., Roldin, P., Berndt, T., Crounse, J. D., Wennberg, P. O., Mentel, T. F., Wildt, J., Junninen, H., Jokinen, T., Kulmala, M., Worsnop, D. R., Thornton, J. A., Donahue, N., Kjaergaard, H. G., and Ehn, M.: Highly Oxygenated Organic Molecules (HOM) from Gas-Phase Autoxidation Involving Peroxy Radicals: A Key Contributor to Atmospheric Aerosol, Chem. Rev., 119, 3472-3509, 10.1021/acs.chemrev.8b00395, 2019.

Boyd, C. M., Sanchez, J., Xu, L., Eugene, A. J., Nah, T., Tuet, W. Y., Guzman, M. I., and Ng, N. L.: Secondary organic aerosol formation from the β-pinene+NO_3 system: effect of humidity and peroxy radical fate, Atmos. Chem. Phys., 15, 7497-7522, 10.5194/acp-15-7497-2015, 2015.

Brown, S. S. and Stutz, J.: Nighttime radical observations and chemistry, Chem. Soc. Rev., 41, 10.1039/c2cs35181a, 2012.

Claflin, M. S., Krechmer, J. E., Hu, W., Jimenez, J. L., and Ziemann, P. J.: Functional Group Composition of Secondary Organic Aerosol Formed from Ozonolysis of α-Pinene Under High VOC and Autoxidation Conditions, ACS Earth Space Chem., 2, 1196-1210, 10.1021/acsearthspacechem.8b00117, 2018.

Daumit, K. E., Kessler, S. H., and Kroll, J. H.: Average chemical properties and potential formation pathways of highly oxidized organic aerosol, Faraday Discuss., 165, 10.1039/c3fd00045a, 2013.

Donahue, N. M., Epstein, S. A., Pandis, S. N., and Robinson, A. L.: A two-dimensional volatility basis set: 1. organic-aerosol mixing thermodynamics, Atmos. Chem. Phys., 11, 3303-3318, 10.5194/acp-11-3303-2011, 2011.

Donahue, N. M., Henry, K. M., Mentel, T. F., Kiendler-Scharr, A., Spindler, C., Bohn, B., Brauers, T., Dorn, H. P., Fuchs, H., Tillmann, R., Wahner, A., Saathoff, H., Naumann, K.-H., Möhler, O., Leisner,

469   T., Müller, L., Reinnig, M.-C., Hoffmann, T., Salo, K., Hallquist, M., Frosch, M., Bilde, M.,
470   Tritscher, T., Barmet, P., Praplan, A. P., DeCarlo, P. F., Dommen, J., Prévôt, A. S. H., and
471   Baltensperger, U.: Aging of biogenic secondary organic aerosol via gas-phase OH radical reactions,
472   P. Natl. Acad. Sci. USA, 109, 13503-13508, 10.1073/pnas.1115186109, 2012.

473 Ehn, M., Thornton, J. A., Kleist, E., Sipilä, M., Junninen, H., Pullinen, I., Springer, M., Rubach, F.,
474   Tillmann, R., and Lee, B.: A large source of low-volatility secondary organic aerosol, Nature, 506,
475   476-479, 2014.

476 Faloona, I., Tan, D., Brune, W., Hurst, J., Barket, D., Couch, T. L., Shepson, P., Apel, E., Riemer, D.,
477   Thornberry, T., Carroll, M. A., Sillman, S., Keeler, G. J., Sagady, J., Hooper, D., and Paterson, K.:
478   Nighttime observations of anomalously high levels of hydroxyl radicals above a deciduous forest
479   canopy, J. Geophys. Res.-Atmos., 106, 24315-24333, 10.1029/2000jd900691, 2001.

480 Fry, J. L., Draper, D. C., Barsanti, K. C., Smith, J. N., Ortega, J., Winkler, P. M., Lawler, M. J., Brown,
481   S. S., Edwards, P. M., Cohen, R. C., and Lee, L.: Secondary organic aerosol formation and organic
482   nitrate yield from NO_3 oxidation of biogenic hydrocarbons, Environ. Sci. Technol., 48, 11944-11953,
483   10.1021/es502204x, 2014.

484 Geyer, A., Bächmann, K., Hofzumahaus, A., Holland, F., Konrad, S., Klüpfel, T., Pätz, H. W., Perner, D.,
485   Mihelcic, D., Schäfer, H. J., Volz-Thomas, A., and Platt, U.: Nighttime formation of peroxy and
486   hydroxyl radicals during the BERLIOZ campaign: Observations and modeling studies, J. Geophys.
487   Res.-Atmos., 108, 10.1029/2001jd000656, 2003a.

488 Geyer, A., Bächmann, K., Hofzumahaus, A., Holland, F., Konrad, S., Klüpfel, T., Pätz, H. W., Perner, D.,
489   Mihelcic, D., Schäfer, H. J., Volz-Thomas, A., and Platt, U.: Nighttime formation of peroxy and
490   hydroxyl radicals during the BERLIOZ campaign: Observations and modeling studies, J. Geophys.
491   Res.-Atmos., 108, 10.1029/2001jd000656, 2003b.

492 Hakola, H., Hellén, H., Hemmilä, M., Rinne, J., and Kulmala, M.: In situ measurements of volatile
493   organic compounds in a boreal forest, Atmos. Chem. Phys., 12, 11665-11678, 10.5194/acp-12-
494   11665-2012, 2012.

495 Hallquist, M., Wängberg, I., Ljungström, E., Barnes, I., and Becker, K. H.: Aerosol and product yields
496   from NO_3 radical-initiated oxidation of selected monoterpenes, Environ. Sci. Technol., 33, 553-559,
497   10.1021/es980292s, 1999.

498 Huang, R. J., Zhang, Y., Bozzetti, C., Ho, K. F., Cao, J. J., Han, Y., Daellenbach, K. R., Slowik, J. G.,
499   Platt, S. M., Canonaco, F., Zotter, P., Wolf, R., Pieber, S. M., Bruns, E. A., Crippa, M., Ciarelli, G.,
500   Piazzalunga, A., Schwikowski, M., Abbaszade, G., Schnelle-Kreis, J., Zimmermann, R., An, Z.,
501   Szidat, S., Baltensperger, U., El Haddad, I., and Prevot, A. S.: High secondary aerosol contribution
502   to particulate pollution during haze events in China, Nature, 514, 218-222, 10.1038/nature13774,
503   2014.

504 Huang, W., Saathoff, H., Shen, X., Ramisetty, R., Leisner, T., and Mohr, C.: Chemical Characterization
505   of Highly Functionalized Organonitrates Contributing to Night-Time Organic Aerosol Mass
506   Loadings and Particle Growth, Environ. Sci. Technol., 53, 1165-1174, 10.1021/acs.est.8b05826,
507   2019.

508 Inomata, S.: New Particle Formation Promoted by OH Reactions during α-Pinene Ozonolysis, ACS Earth
509   Space Chem., 5, 1929-1933, 10.1021/acsearthspacechem.1c00142, 2021.

510 Isaacman-VanWertz, G. and Aumont, B.: Impact of organic molecular structure on the estimation of
511   atmospherically relevant physicochemical parameters, Atmos. Chem. Phys., 21, 6541-6563,
512   10.5194/acp-21-6541-2021, 2021.

513   Iyer, S., Rissanen, M. P., Valiev, R., Barua, S., Krechmer, J. E., Thornton, J., Ehn, M., and Kurten, T.:
514   Molecular mechanism for rapid autoxidation in alpha-pinene ozonolysis, Nat. Commun., 12, 878,
515   10.1038/s41467-021-21172-w, 2021.

516   Jenkin, M., Young, J., and Rickard, A.: The MCM v3.3.1 degradation scheme for isoprene, Atmos. Chem.
517   Phys., 15, 11433-11459, https://doi.org/10.5194/acp-15-11433-2015, 2015.

518   Jokinen, T., Sipilä, M., Richters, S., Kerminen, V. M., Paasonen, P., Stratmann, F., Worsnop, D., Kulmala,
519   M., Ehn, M., and Herrmann, H.: Rapid autoxidation forms highly oxidized RO_2 radicals in the
520   atmosphere, Angew. Chem. Int. Ed., 53, 14596-14600, 2014.

521   Junninen, H., Ehn, M., Petäjä, T., Luosujärvi, L., Kotiaho, T., Kostiainen, R., Rohner, U., Gonin, M.,
522   Fuhrer, K., Kulmala, M., andWorsnop, D. R.: A high-resolution mass spectrometer to measure
523   atmospheric ion composition, Atmos. Meas. Tech., 3, 1039–1053, https://doi.org/10.5194/amt-3-
524   1039-2010, 2010.

525   Junninen, H., Hulkkonen, M., Riipinen, I., Nieminen, T., Hirsikko, A., Suni, T., Boy, M., Lee, S.-H.,
526   Vana, M., Tammet, H., Kerminen, V.-M., and Kulmala, M.: Observations on nocturnal growth of
527   atmospheric clusters, Tellus B: Chemical and Physical Meteorology, 60, 10.1111/j.1600-
528   0889.2008.00356.x, 2017.

529   Kenseth, C. M., Huang, Y., Zhao, R., Dalleska, N. F., Hethcox, J. C., Stoltz, B. M., and Seinfeld, J. H.:
530   Synergistic O_3 + OH oxidation pathway to extremely low-volatility dimers revealed in beta-pinene
531   secondary organic aerosol, P. Natl. Acad. Sci. USA, 115, 8301-8306, 10.1073/pnas.1804671115,
532   2018.

533   Kirkby, J., Duplissy, J., Sengupta, K., Frege, C., Gordon, H., Williamson, C., Heinritzi, M., Simon, M.,
534   Yan, C., Almeida, J., Tröstl, J., Nieminen, T., Ortega, I. K., Wagner, R., Adamov, A., Amorim, A.,
535   Bernhammer, A.-K., Bianchi, F., Breitenlechner, M., Brilke, S., Chen, X., Craven, J., Dias, A.,
536   Ehrhart, S., Flagan, R. C., Franchin, A., Fuchs, C., Guida, R., Hakala, J., Hoyle, C. R., Jokinen, T.,
537   Junninen, H., Kangasluoma, J., Kim, J., Krapf, M., Kürten, A., Laaksonen, A., Lehtipalo, K.,
538   Makhmutov, V., Mathot, S., Molteni, U., Onnela, A., Peräkylä, O., Piel, F., Petäjä, T., Praplan, A. P.,
539   Pringle, K., Rap, A., Richards, N. A. D., Riipinen, I., Rissanen, M. P., Rondo, L., Sarnela, N.,
540   Schobesberger, S., Scott, C. E., Seinfeld, J. H., Sipilä, M., Steiner, G., Stozhkov, Y., Stratmann, F.,
541   Tomé, A., Virtanen, A., Vogel, A. L., Wagner, A. C., Wagner, P. E., Weingartner, E., Wimmer, D.,
542   Winkler, P. M., Ye, P., Zhang, X., Hansel, A., Dommen, J., Donahue, N. M., Worsnop, D. R.,
543   Baltensperger, U., Kulmala, M., Carslaw, K. S., and Curtius, J.: Ion-induced nucleation of pure
544   biogenic particles, Nature, 533, 521-526, 10.1038/nature17953, 2016.

545   Kristensen, K., Watne, Å. K., Hammes, J., Lutz, A., Petäjä, T., Hallquist, M., Bilde, M., and Glasius, M.:
546   High-Molecular Weight Dimer Esters Are Major Products in Aerosols from α-Pinene Ozonolysis
547   and the Boreal Forest, Environ. Sci. Tech. Let., 3, 280-285, 10.1021/acs.estlett.6b00152, 2016.

548   Kulmala, M., Hämeri, K., Aalto, P. P., Mäkelä, J. M., Pirjola, L., Nilsson, E. D., Buzorius, G., Rannik,
549   Ü., Dal Maso, M., Seidl, W., Hoffman, T., Janson, R., Hansson, H. C., Viisanen, Y., Laaksonen, A.,
550   and O'Dowd, C. D.: Overview of the international project on biogenic aerosol formation in the
551   boreal forest (BIOFOR), Tellus Series B-Chemical and Physical Meteorology, 53, 324-343,
552   10.1034/j.1600-0889.2001.530402.x, 2001.

553   Kurtén, T., Møller, K. H., Nguyen, T. B., Schwantes, R. H., Misztal, P. K., Su, L., Wennberg, P. O., Fry,
554   J. L., and Kjaergaard, H. G.: Alkoxy Radical Bond Scissions Explain the Anomalously Low
555   Secondary Organic Aerosol and Organonitrate Yields From α-Pinene + NO_3, J. Phys. Chem. Lett.,
556   8, 2826-2834, 10.1021/acs.jpclett.7b01038, 2017.

557 Lee, B. H., D'Ambro, E. L., Lopez-Hilfiker, F. D., Schobesberger, S., Mohr, C., Zawadowicz, M. A., Liu,
558 J., Shilling, J. E., Hu, W., Palm, B. B., Jimenez, J. L., Hao, L., Virtanen, A., Zhang, H., Goldstein,
559 A. H., Pye, H. O. T., and Thornton, J. A.: Resolving ambient organic aerosol formation and aging
560 pathways with simultaneous molecular composition and volatility observations, ACS Earth Space
561 Chem., 4, 391-402, 10.1021/acsearthspacechem.9b00302, 2020.
562 Lee, S. H., Uin, J., Guenther, A. B., de Gouw, J. A., Yu, F., Nadykto, A. B., Herb, J., Ng, N. L., Koss, A.,
563 Brune, W. H., Baumann, K., Kanawade, V. P., Keutsch, F. N., Nenes, A., Olsen, K., Goldstein, A.,
564 and Ouyang, Q.: Isoprene suppression of new particle formation: Potential mechanisms and
565 implications, J. Geophys. Res.-Atmos., 121, 10.1002/2016jd024844, 2016.
566 Li, D., Huang, W., Wang, D., Wang, M., Thornton, J. A., Caudillo, L., Rörup, B., Marten, R., Scholz, W.,
567 Finkenzeller, H., Marie, G., Baltensperger, U., Bell, D. M., Brasseur, Z., Curtius, J., Dada, L.,
568 Duplissy, J., Gong, X., Hansel, A., He, X.-C., Hofbauer, V., Junninen, H., Krechmer, J. E., Kürten,
569 A., Lamkaddam, H., Lehtipalo, K., Lopez, B., Ma, Y., Mahfouz, N. G. A., Manninen, H. E., Mentler,
570 B., Perrier, S., Petäjä, T., Pfeifer, J., Philippov, M., Schervish, M., Schobesberger, S., Shen, J., Surdu,
571 M., Tomaz, S., Volkamer, R., Wang, X., Weber, S. K., Welti, A., Worsnop, D. R., Wu, Y., Yan, C.,
572 Zauner-Wieczorek, M., Kulmala, M., Kirkby, J., Donahue, N. M., George, C., El-Haddad, I.,
573 Bianchi, F., and Riva, M.: Nitrate Radicals Suppress Biogenic New Particle Formation from
574 Monoterpene Oxidation, Environ. Sci. Technol., 10.1021/acs.est.3c07958, 2024.
575 Li, Y., Pöschl, U., and Shiraiwa, M.: Molecular corridors and parameterizations of volatility in the
576 chemical evolution of organic aerosols, Atmos. Chem. Phys., 16, 3327-3344, 10.5194/acp-16-3327-
577 2016, 2016.
578 Liebmann, J., Karu, E., Sobanski, N., Schuladen, J., Ehn, M., Schallhart, S., Quéléver, L., Hellen, H.,
579 Hakola, H., Hoffmann, T., Williams, J., Fischer, H., Lelieveld, J., and Crowley, J. N.: Direct
580 measurement of NO₃ radical reactivity in a boreal forest, Atmos. Chem. Phys., 18, 3799-3815,
581 10.5194/acp-18-3799-2018, 2018.
582 Liu, J., D'Ambro, E. L., Lee, B. H., Schobesberger, S., Bell, D. M., Zaveri, R. A., Zelenyuk, A., Thornton,
583 J. A., and Shilling, J. E.: Monoterpene Photooxidation in a Continuous-Flow Chamber: SOA Yields
584 and Impacts of Oxidants, NO(x), and VOC Precursors, Environ. Sci. Technol., 56, 12066-12076,
585 10.1021/acs.est.2c02630, 2022.
586 Mentel, T., Springer, M., Ehn, M., Kleist, E., Pullinen, I., Kurtén, T., Rissanen, M., Wahner, A., and Wildt,
587 J.: Formation of highly oxidized multifunctional compounds: autoxidation of peroxy radicals
588 formed in the ozonolysis of alkenes–deduced from structure–product relationships, Atmos. Chem.
589 Phys., 15, 6745-6765, 2015.
590 Mohr, C., Lopez-Hilfiker, F. D., Yli-Juuti, T., Heitto, A., Lutz, A., Hallquist, M., D'Ambro, E. L.,
591 Rissanen, M. P., Hao, L., Schobesberger, S., Kulmala, M., Mauldin, R. L., Makkonen, U., Sipilä,
592 M., Petäjä, T., and Thornton, J. A.: Ambient observations of dimers from terpene oxidation in the
593 gas phase: Implications for new particle formation and growth, Geophys. Res. Lett., 44, 2958-2966,
594 10.1002/2017gl072718, 2017.
595 Mutzel, A., Zhang, Y., Böge, O., Rodigast, M., Kolodziejczyk, A., Wang, X., and Herrmann, H.:
596 Importance of secondary organic aerosol formation of α-pinene, limonene, and m-cresol comparing
597 day- and nighttime radical chemistry, Atmos. Chem. Phys., 21, 8479-8498, 10.5194/acp-21-8479-
598 2021, 2021.
599 Nguyen, T. B., Crounse, J. D., Teng, A. P., St. Clair, J. M., Paulot, F., Wolfe, G. M., and Wennberg, P. O.:
600 Rapid deposition of oxidized biogenic compounds to a temperate forest, P. Natl. Acad. Sci. USA,

601 112, 10.1073/pnas.1418702112, 2015.

602 Perraud, V., Bruns, E. A., Ezell, M. J., Johnson, S. N., Greaves, J., and Finlayson-Pitts*, B. J.:
603 Identification of Organic Nitrates in the NO_3 Radical Initiated Oxidation of r-Pinene by
604 Atmospheric Pressure Chemical Ionization MassSpectrometry, Environ. Sci. Technol., 44, 5887–
605 5893, 2010.

606 Pye, H. O. T., Ward-Caviness, C. K., Murphy, B. N., Appel, K. W., and Seltzer, K. M.: Secondary organic
607 aerosol association with cardiorespiratory disease mortality in the United States, Nat. Commun., 12,
608 10.1038/s41467-021-27484-1, 2021.

609 Schervish, M. and Donahue, N. M.: Peroxy radical chemistry and the volatility basis set, Atmos. Chem.
610 Phys., 20, 1183-1199, 10.5194/acp-20-1183-2020, 2020.

611 Shen, H., Vereecken, L., Kang, S., Pullinen, I., Fuchs, H., Zhao, D., and Mentel, T. F.: Unexpected
612 significance of a minor reaction pathway in daytime formation of biogenic highly oxygenated
613 organic compounds, Sci. Adv., 8, eabp8702, 10.1126/sciadv.abp8702, 2022.

614 Shrivastava, M., Cappa, C. D., Fan, J., Goldstein, A. H., Guenther, A. B., Jimenez, J. L., Kuang, C.,
615 Laskin, A., Martin, S. T., Ng, N. L., Petaja, T., Pierce, J. R., Rasch, P. J., Roldin, P., Seinfeld, J. H.,
616 Shilling, J., Smith, J. N., Thornton, J. A., Volkamer, R., Wang, J., Worsnop, D. R., Zaveri, R. A.,
617 Zelenyuk, A., and Zhang, Q.: Recent advances in understanding secondary organic aerosol:
618 Implications for global climate forcing, Rev. Geophy., 55, 509-559, 10.1002/2016rg000540, 2017.

619 Simon, M., Dada, L., Heinritzi, M., Scholz, W., Stolzenburg, D., Fischer, L., Wagner, A. C., Kürten, A.,
620 Rörup, B., He, X.-C., Almeida, J., Baalbaki, R., Baccarini, A., Bauer, P. S., Beck, L., Bergen, A.,
621 Bianchi, F., Bräkling, S., Brilke, S., Caudillo, L., Chen, D., Chu, B., Dias, A., Draper, D. C., Duplissy,
622 J., El-Haddad, I., Finkenzeller, H., Frege, C., Gonzalez-Carracedo, L., Gordon, H., Granzin, M.,
623 Hakala, J., Hofbauer, V., Hoyle, C. R., Kim, C., Kong, W., Lamkaddam, H., Lee, C. P., Lehtipalo,
624 K., Leiminger, M., Mai, H., Manninen, H. E., Marie, G., Marten, R., Mentler, B., Molteni, U.,
625 Nichman, L., Nie, W., Ojdanic, A., Onnela, A., Partoll, E., Petäjä, T., Pfeifer, J., Philippov, M.,
626 Quéléver, L. L. J., Ranjithkumar, A., Rissanen, M. P., Schallhart, S., Schobesberger, S., Schuchmann,
627 S., Shen, J., Sipilä, M., Steiner, G., Stozhkov, Y., Tauber, C., Tham, Y. J., Tomé, A. R., Vazquez-
628 Pufleau, M., Vogel, A. L., Wagner, R., Wang, M., Wang, D. S., Wang, Y., Weber, S. K., Wu, Y., Xiao,
629 M., Yan, C., Ye, P., Ye, Q., Zauner-Wieczorek, M., Zhou, X., Baltensperger, U., Dommen, J., Flagan,
630 R. C., Hansel, A., Kulmala, M., Volkamer, R., Winkler, P. M., Worsnop, D. R., Donahue, N. M.,
631 Kirkby, J., and Curtius, J.: Molecular understanding of new-particle formation from α-pinene
632 between −50 and +25 °C, Atmos. Chem. Phys., 20, 9183-9207, 10.5194/acp-20-9183-2020, 2020.

633 Stone, D., Whalley, L. K., and Heard, D. E.: Tropospheric OH and HO_2 radicals: field measurements and
634 model comparisons, Chem. Soc. Rev., 41, 10.1039/c2cs35140d, 2012.

635 Wang, Y., Zhao, Y., Li, Z., Li, C., Yan, N., and Xiao, H.: Importance of Hydroxyl Radical Chemistry in
636 Isoprene Suppression of Particle Formation from α-Pinene Ozonolysis, ACS Earth Space Chem., 5,
637 487-499, 10.1021/acsearthspacechem.0c00294, 2021.

638 Wolfe, G. M., Marvin, M. R., Roberts, S. J., Travis, K. R., and Liao, J.: The framework for 0-D
639 atmospheric modeling (F0AM) v3. 1, Geosci. Model Dev., 9, 3309-3319,
640 https://doi.org/10.5194/gmd-9-3309-2016, 2016.

641 Xu, L., Møller, K. H., Crounse, J. D., Otkjær, R. V., Kjaergaard, H. G., and Wennberg, P. O.:
642 Unimolecular Reactions of Peroxy Radicals Formed in the Oxidation of α-Pinene and β-Pinene by
643 Hydroxyl Radicals, J. Phys. Chem. A, 123, 1661-1674, 10.1021/acs.jpca.8b11726, 2019.

644 Zang, H., Huang, D., Zhong, J., Li, Z., Li, C., Xiao, H., and Zhao, Y.: Direct probing of acylperoxy

645   radicals during ozonolysis of α-pinene: constraints on radical chemistry and production of highly
646   oxygenated organic molecules, Atmos. Chem. Phys., 23, 12691-12705, 10.5194/acp-23-12691-
647   2023, 2023.

648 Zhang, H., Yee, L. D., Lee, B. H., Curtis, M. P., Worton, D. R., Isaacman-VanWertz, G., Offenberg, J. H.,
649   Lewandowski, M., Kleindienst, T. E., Beaver, M. R., Holder, A. L., Lonneman, W. A., Docherty, K.
650   S., Jaoui, M., Pye, H. O. T., Hu, W., Day, D. A., Campuzano-Jost, P., Jimenez, J. L., Guo, H., Weber,
651   R. J., de Gouw, J., Koss, A. R., Edgerton, E. S., Brune, W., Mohr, C., Lopez-Hilfiker, F. D., Lutz,
652   A., Kreisberg, N. M., Spielman, S. R., Hering, S. V., Wilson, K. R., Thornton, J. A., and Goldstein,
653   A. H.: Monoterpenes are the largest source of summertime organic aerosol in the southeastern
654   United States, P. Natl. Acad. Sci. USA, 115, 2038-2043, 10.1073/pnas.1717513115, 2018.

655 Zhang, Y., Peräkylä, O., Yan, C., Heikkinen, L., Äijälä, M., Daellenbach, K. R., Zha, Q., Riva, M.,
656   Garmash, O., Junninen, H., Paatero, P., Worsnop, D., and Ehn, M.: Insights into atmospheric
657   oxidation processes by performing factor analyses on subranges of mass spectra, Atmos. Chem.
658   Phys., 20, 5945-5961, 10.5194/acp-20-5945-2020, 2020.

659 Zhao, Y., Thornton, J. A., and Pye, H. O. T.: Quantitative constraints on autoxidation and dimer formation
660   from direct probing of monoterpene-derived peroxy radical chemistry, P. Natl. Acad. Sci. USA, 115,
661   12142-12147, 10.1073/pnas.1812147115, 2018.

662 Zhao, Y., Yao, M., Wang, Y., Li, Z., Wang, S., Li, C., and Xiao, H.: Acylperoxy Radicals as Key
663   Intermediates in the Formation of Dimeric Compounds in α-Pinene Secondary Organic Aerosol,
664   Environ. Sci. Technol., 56, 14249-14261, 2022.

665 Zhao, Z., Zhang, W., Alexander, T., Zhang, X., Martin, D. B. C., and Zhang, H.: Isolating alpha-Pinene
666   Ozonolysis Pathways Reveals New Insights into Peroxy Radical Chemistry and Secondary Organic
667   Aerosol Formation, Environ. Sci. Technol., 55, 6700-6709, 10.1021/acs.est.1c02107, 2021.

668